# Coupling of Edge States and Topological Bragg Solitons

Weifeng Zhang,[1] Xianfeng Chen,[1] Yaroslav V. Kartashov,[2] Vladimir V. Konotop,[3] and Fangwei Ye[1,*]
[1]State Key Laboratory of Advanced Optical Communication Systems and Networks, School of Physics and Astronomy, Shanghai Jiao Tong University, Shanghai 200240, China
[2]Institute of Spectroscopy, Russian Academy of Sciences, Troitsk, Moscow Region, 108840, Russia
[3]Departamento de Física and Centro de Física Teórica e Computacional, Faculdade de Ciências, Universidade de Lisboa, Campo Grande, Edifício C8, Lisboa 1749-016, Portugal

(Received 18 May 2019; published 19 December 2019)

The existence of the edge states at the interface between two media with different topological properties is protected by symmetry, which makes such states robust against structural defects or disorder. We show that, if a system supports more than one topological edge state at the interface, even a weak periodic deformation may scatter one edge state into another without coupling to bulk modes. This is the Bragg scattering of the edge modes, which in a topological system is highly selective, with closed bulk and backward scattering channels, even when conditions for resonant scattering are not satisfied. When such a system bears nonlinearity, Bragg scattering enables the formation of a new type of soliton—topological Bragg solitons. We report them in a spin-orbit-coupled (SOC) Bose-Einstein condensate in a homogeneous honeycomb Zeeman lattice. An interface supporting two edge states is created by two different SOCs, with the $y$ component of the synthetic magnetic field having opposite directions at different sides of the interface. The reported Bragg solitons are found to be stable.

DOI: 10.1103/PhysRevLett.123.254103

Topological edge states are fundamental for understanding the physics of many phenomena including quantum [1,2], anomalous [3], and quantum spin [4,5] Hall effects, topological insulators [6], Majorana fermions [7], just to mention a few. Introduced in solid state physics, topological edge states were shown to be a universal wave phenomenon. In particular, they enable protected edge currents in photonic crystals as predicted in [8] and observed in [9–11] (see review [12]), in surface plasmon-polariton systems [13], in systems of cold atoms in optical lattices [14–16], in spin-orbit coupled Bose-Einstein condensates (SOC BECs) [17], and in optoelectronic systems, such as exciton-polariton condensates [18,19].

Topological edge states are robust against disorder [6], which distinguishes them from bulk states that can be manipulated by perturbations [20]. This makes such states promising for a variety of applications. Meanwhile, when it is necessary to selectively excite or remove edge states, or transform them in any other way, this robustness becomes a drawback. Topological edge states can be coupled by nonlinearity that gives rise to a rich set of phenomena, such as modulation instability [19] or envelope soliton propagating along the edge [17]. However, by enabling *linear* coupling one qualitatively enriches the physics of respective systems. Now nonlinear interactions, requiring simultaneous energy and momentum conservation laws, can be made resonant. That leads to a plethora of novel phenomena, which so far were not considered for edge states. In particular, linear mode coupling resulting from periodic modulation of the system, i.e., from Bragg scattering, in the presence of nonlinearity can lead to the formation of Bragg solitons [21,22], which are relevant for many applications [23], and whose properties qualitatively differ from those of the envelope solitons mentioned above.

In this Letter, we introduce an efficient mechanism of coupling and conversion of topological edge states based on Bragg scattering by periodic modulations of an interface between topologically different media. This mechanism works when a system supports more than one topological edge state per interface. We show that even a very weak periodic perturbation of such an interface may result in periodic transitions between two edge states moving with different group velocities. Such a coupling is highly selective, with closed bulk and backward scattering channels. Furthermore, we construct Bragg solitons propagating along the interface and representing a spatially localized envelope of two coupled edge states.

As a case example, we address an atomic SOC BEC [24,25], characterized by a spinor order parameter $\mathbf{\Psi} = (\Psi^{(1)}, \Psi^{(2)})^T$ ($T$ stands for the transpose). The condensate is placed in a honeycomb lattice, which can be created experimentally by applying at least three laser beams [26,27]. Almost arbitrary 2D field distributions, and thus optical potentials, can be produced by the interference of quasinondiffracting laser beams [28]. The lattice is characterized by inverted potential profiles for the spinor components and can be created by periodically varying Zeeman splitting (see [29] for a possibility of experimental

 

realization). Below such potential is termed a Zeeman lattice (ZL). The interface supporting edge states is created by two different spin-orbit couplings (SOCs). Although we focus on SO BECs, our findings can be extended to any system supporting several topological edge states per interface, including gyromagnetic photonic crystals [9], polariton microcavities [18], and photonic waveguide arrays [30].

The ZL is simulated by the matrix potential $\sigma_z R(\boldsymbol{r})$, where $R(\boldsymbol{r})$ is a periodic function and $(\sigma_x, \sigma_y, \sigma_z) = \boldsymbol{\sigma}$ are the Pauli matrices. The respective linear part of the Hamiltonian is $H_{\rm latt} = \boldsymbol{p}^2/2 + \sigma_z R(\boldsymbol{r})$, where $\boldsymbol{p} = (-i\partial_x, -i\partial_y)$ is the momentum operator (in the units, where $\hbar = m = 1$). We consider $R(\boldsymbol{r}) \leq 0$; i.e., the ZL acts as an array of potential wells and a barrier for the components $\Psi^{(1)}$ and $\Psi^{(2)}$, respectively. This results in the dominance of $\Psi^{(1)}$ component in states with negative energies. In a sufficiently deep ZL, when the coupling to the $\Psi^{(2)}$ component is a weak perturbation for the $\Psi^{(1)}$ component, the properties of the lowest gap are determined by the topology of the Dirac points of the conventional honeycomb lattice [31] (for previous studies of BECs in discrete honeycomb lattices see also [27,32]). Thus, when a ZL has a boundary with uniform media, the application of SOC enables topological edge states [17].

If a ZL is infinite, a space-dependent SOC by itself can create an interface supporting topological states. Indeed, assume that Rashba SOC [33], $H_R = \beta(p_y\sigma_x - p_x\sigma_y)$, and Dresselhaus SOC [34], $H_D = -\beta(p_x\sigma_y + p_y\sigma_x)$, of equal strengths $\beta$, are induced in the left ($x < 0$) and in the right ($x > 0$) half-spaces, respectively. The SOC Hamiltonian can be written as $H_{\rm SOC} = -\beta[p_x\sigma_y + \chi(x)p_y\sigma_x]$, where $\chi(x) \equiv \mathrm{sign}(x)$ [note that $\chi(x)$ here can be replaced by any smooth function, whose transition region between $-1$ and $+1$ is less than the lattice period in the $x$ direction]. The resulting linear Hamiltonian acquires the form $H_0 = H_{\rm latt} + H_{\rm SOC}$. The Rashba SOC acting in the bulk ZL (the Hamiltonian $H_{\rm latt} + H_R$) breaks time-reversal symmetry and opens the topological gap between the two lowest bands characterized by the Chern numbers $C_1 = -1$ and $C_2 = 1$. In contrast, Dresselhaus SOC acting in the bulk ZL (the Hamiltonian $H_{\rm latt} + H_D$) results in $C_1 = 1$ and $C_2 = -1$ Chern numbers of the two lowest bands. Thus, a SOC interface created at $x = 0$ supports two edge states, since the difference of the gap Chern numbers [2] of the lattices at $x < 0$ and $x > 0$ is 2. This is shown in Fig. 1(a) for a honeycomb ZL illustrated in Fig. 1(b).

The interface breaks the translational symmetry along the $x$ axis, but the system remains $L$ periodic along the $y$ axis, i.e., $R(\boldsymbol{r} + L\hat{\boldsymbol{j}}) = R(\boldsymbol{r})$ (for the hexagonal lattice $L = \sqrt{3}a$, where $a$ is the distance between neighboring sites). Consider two orthonormal edge states, $\boldsymbol{\psi}_j = (\psi_j^{(1)}, \psi_j^{(2)})^T$, $j = 1, 2$, corresponding to an energy $\varepsilon_0$, i.e., $H_0\boldsymbol{\psi}_{1,2} = \varepsilon_0\boldsymbol{\psi}_{1,2}$, but different Bloch momenta $k_{1,2}$ in the $y$ direction (like the states shown in Fig. 1). Because of the Bloch theorem $\boldsymbol{\psi}_j(\boldsymbol{r}) = e^{ik_j y}\boldsymbol{u}_j(x,y)$, where $\boldsymbol{u}_j(x,y) = \boldsymbol{u}_j(x,y+L)$. One has $[H_{\rm latt}, \mathcal{P}_{x,y}] = 0$, where $\mathcal{P}_x$ and $\mathcal{P}_y$ are the operators performing inversions $x \to -x$ and $y \to -y$, respectively. One also obtains $[H_0, \sigma_z\mathcal{P}_x] = [H_0, \mathcal{P}_y\mathcal{K}] = 0$, where $\mathcal{K}$ is the complex conjugation. The symmetry $\mathcal{P}_y\mathcal{K}$ implies that $\boldsymbol{u}_j(x,y) = e^{-i\varphi_j}\boldsymbol{u}_j^*(x,-y)$, where $\varphi_j$ is an arbitrary constant phase. Since $\sigma_z\mathcal{P}_x\boldsymbol{u}_j = \pm\boldsymbol{u}_j$, the components of a spinor $\boldsymbol{u}_j$ have opposite parities with respect to $x$.

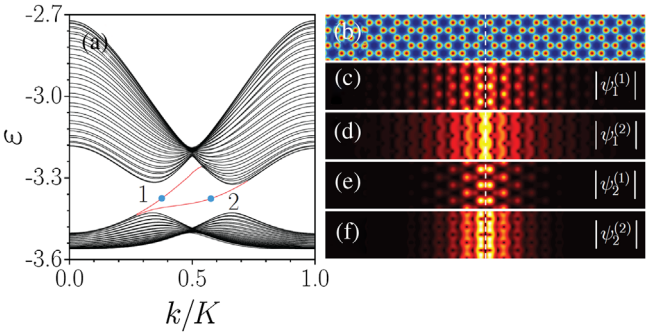


FIG. 1. (a) Two lowest bands in the spectrum of the ZL with $R(\boldsymbol{r}) = -\rho\sum_{m,n}\exp[-(\boldsymbol{r} - \boldsymbol{r}_{mn})^2/d^2]$ shown in (b) for one component. The amplitude of the lattice is $\rho = 8$, the characteristic width of the potential maxima and minima centered at the nodes $\boldsymbol{r}_{mn} = (x_m, y_n)$ of the honeycomb grid is $d = 0.5$, the distance between neighboring sites is $a = 1.4$. The dashed line in (b) indicates the interface between domains with Rashba SOC (left) and Dresselhaus SOC (right) with equal amplitudes $\beta = 1.5$. Moduli of the components of the edge state 1 at $k_1 = 0.375K$ (c),(d) and of the edge state 2 at $k_2 = 0.575K$ (e),(f), where $K = 2\pi/\sqrt{3}a$. Both states, marked by the blue dots in (a), have the energy $\varepsilon_0 \approx -3.376$.

Further, we take into account that the modes 1 and 2 belong to two neighboring branches of the dispersion relation (i.e., for any given $k$ in the Brillouin zone these are subsequent energy levels). Since the symmetry of a mode holds along the dispersion curve and there are only two noncrossing edge states in the topological gap, one conjectures that the $\sigma_z\mathcal{P}_x$ symmetries of the states $\boldsymbol{\psi}_{1,2}(\boldsymbol{r})$ are different. In other words, the same spinor components of the edge states 1 and 2, have different parity in $x$. These considerations are consistent with the symmetry of numerically calculated modes, shown in Figs. 1(c)–1(f), for which $\mathcal{P}_x\psi_j^{(\alpha)} = (-1)^{j+\alpha+1}\psi_j^{(\alpha)}$. This also ensures mutual orthogonality of the edge states allowing us to choose them to satisfy ($j$, $l = 1$, 2): $\langle\boldsymbol{\psi}_j|\boldsymbol{\psi}_l\rangle = \delta_{jl}$, where we define $\langle\boldsymbol{\psi}_j|\mathcal{O}|\boldsymbol{\psi}_l\rangle = \int_{-\infty}^{\infty}dx\int_0^L dy\boldsymbol{\psi}_j^\dagger\mathcal{O}\boldsymbol{\psi}_l$ for an observable $\mathcal{O}$. These properties have implications for the averaged values of the pseudospin $\boldsymbol{s}_j = \langle\boldsymbol{\psi}_j|\boldsymbol{\sigma}|\boldsymbol{\psi}_j\rangle = (s_{x,j}, s_{y,j}, s_{z,j})$: for the $j$th edge state one computes $\boldsymbol{s}_j = (0, 0, s_{z,j})$. For the states shown in Figs. 1(c)–1(f) we have $s_{z,1} \approx 0.7021$ and $s_{z,2} \approx 0.8012$; i.e., both states are mixed ones: $|s_{z,j}| < 1$.

A weak perturbation $U_d(\boldsymbol{r})$, which is periodic along the interface can *resonantly* couple the edge states, by means of Bragg scattering. This occurs if the quasimomentum and energy conservation laws, alias matching conditions for the exact Bragg resonance, are satisfied simultaneously. For the states with equal energies $\varepsilon_0$, the quasimomentum conservation is achieved if the period of the perturbation $\ell$ is chosen as $\ell = 2\pi/\kappa \gg L$, where $\kappa = k_2^0 - k_1^0 \ll K$ is the lattice constant of the perturbation [we consider $k_1^0 < k_2^0$, see Fig. 1(a), and use the index "0" for a pair of Bloch vectors exactly satisfying the resonance condition]. To determine the $x$ dependence of the $U_d(\boldsymbol{r})$, we recall that the edge states from different branches have opposite parities in the $x$ direction. Hence, the perturbation must be an odd function of $x$, which is centered at the interface and has sufficiently large width $l_d$ to ensure significant overlapping with edge states (thus the symmetry of the states determines the $x$ dependence of the perturbation ensuring the most efficient coupling). Below we use $U_d(\boldsymbol{r}) = \delta\chi(x)R(\boldsymbol{r})\cos(\kappa y)$, for $|x| < l_d/2$ and $U_d(\boldsymbol{r}) \equiv 0$ for $|x| > l_d/2$, where $\delta \ll 1$ is the modulation amplitude.

Now the linear Hamiltonian is given by $H = H_0 + \sigma_z U_d(\boldsymbol{r})$, and taking into account two-body interactions the Gross-Pitaevskii equation for the spinor $\boldsymbol{\Psi}$ takes the form

$$i\partial_t \boldsymbol{\Psi} = H\boldsymbol{\Psi} + g(\boldsymbol{\Psi}^\dagger\boldsymbol{\Psi})\boldsymbol{\Psi}, \tag{1}$$

where $g > 0$ ($g < 0$) for the BEC with positive (negative) scattering length. We are interested in the evolution of a wave packet, prepared at $t = 0$ as a superposition of two edge states $\boldsymbol{\psi}_{1,2}$, $\boldsymbol{\Psi}(\boldsymbol{r}, 0) = a_{01}\boldsymbol{\psi}_1(\boldsymbol{r}) + a_{02}\boldsymbol{\psi}_2(\boldsymbol{r})$, where $a_{0j}$ are complex amplitudes. First, we relax the requirement of the exact matching conditions and consider edge states with the Bloch momenta $k_j = k_j^0 + (-1)^j\Delta k/2$, where $|\Delta k| \ll \kappa$ is a deviation from the exact resonance. The respective energies are given by $\varepsilon_{1,2} = \varepsilon_0 \mp \Delta\varepsilon/2$, where for a small $\Delta k$ one approaches $\Delta\varepsilon \approx (v_1 + v_2)\Delta k/2$, with $|\Delta\varepsilon(k)| \ll \varepsilon_0$ and $v_j = \partial\varepsilon_j(k_j^0)/\partial k_j^0$ being the group velocity of the $j$th state in the exact Bragg resonance. Since the resonant interaction of the edge states dominates over their coupling to bulk modes, at $t > 0$ the wave function is given by $\boldsymbol{\Psi}(\boldsymbol{r}, t) = a_1(t, y)\boldsymbol{\psi}_1 e^{-i\varepsilon_1 t} + a_2(t, y)\boldsymbol{\psi}_2 e^{-i\varepsilon_2 t}$, where the evolution of amplitudes $a_j$ is described by the two-mode model derived from (1) [35]:

$$\begin{aligned} &i\partial_t a_j + iv_j\partial_y a_j - ce^{i(-1)^{j-1}(\Delta k y - \Delta\varepsilon t)}a_{3-j} \\ &\quad - g(\chi_j|a_j|^2 + \tilde{\chi}|a_{3-j}|^2)a_j = 0. \end{aligned} \tag{2}$$

Here, $j = 1, 2$, $c = \delta\langle\boldsymbol{\psi}_1|\chi\sigma_z R|\boldsymbol{\psi}_2\rangle/2$ is the coupling constant (it is real), and the nonlinear coefficients $\chi_j = \langle\boldsymbol{\psi}_j^\dagger\boldsymbol{\psi}_j|\boldsymbol{\psi}_j^\dagger\boldsymbol{\psi}_j\rangle$ and $\tilde{\chi} = \langle\boldsymbol{\psi}_1^\dagger\boldsymbol{\psi}_1|\boldsymbol{\psi}_2^\dagger\boldsymbol{\psi}_2\rangle + \langle\boldsymbol{\psi}_2^\dagger\boldsymbol{\psi}_1|\boldsymbol{\psi}_2^\dagger\boldsymbol{\psi}_1\rangle$ are positive constants.

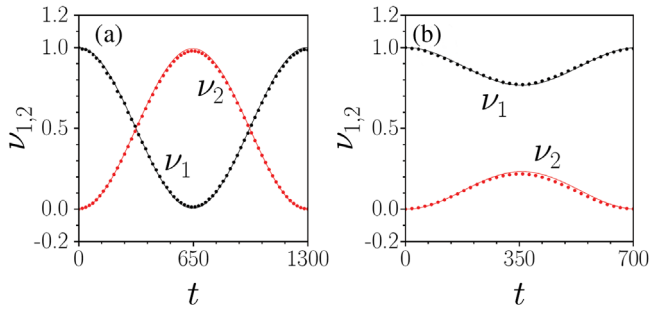


FIG. 2. Linear evolution of $\nu_{1,2}$ in the exact Bragg resonance $\kappa_2 = \kappa_1 + 0.2K$ (a) and near Bragg resonance $\kappa_2 = \kappa_1 + 0.225K$, i.e., $\Delta k = 0.025K$ corresponding to $\Delta\varepsilon = 0.0077$ (b). The dots and solid lines show, respectively, the results of direct solution of Eq. (1) and predictions of the coupled-mode theory. In both cases the modulation depth is $\delta = 0.004$, while at $t = 0$, $\nu_1 = 1$, and $\nu_2 = 0$.

First, we describe linear Bragg scattering of the edge states at $g = 0$. Normalizing the initial amplitudes as $|a_{01}|^2 + |a_{02}|^2 = 1$, and considering the exact Bragg resonance, for $y$-independent amplitudes $a_{1,2}$ one obtains $a_1 = \cos(|c|t + \vartheta_0)$, $a_2 = e^{-i(\pi/2 + \arg c)}\sin(|c|t + \vartheta_0)$, where $\vartheta_0$ is a real constant. In Fig. 2(a) we compare the linear densities of the edge states $\nu_j = |a_j(t)|^2$ obtained from this solution for $\vartheta_0 = 0$ (solid lines) and from the direct simulations of Eq. (1) (dots) where the amplitudes were computed as $a_j(t) = \int_A \boldsymbol{\psi}_j^\dagger(\boldsymbol{r})\boldsymbol{\Psi}(\boldsymbol{r}, t)d\boldsymbol{r}$ with $A$ being the total area of the lattice. As predicted, even weak periodic grating leads to practically complete transition between two edge states. The process is periodic: after atoms transfer into state 2 at $t = \pi/2|c|$ (where $\nu_2 \approx 1$), the reverse transfer starts, so that the initial state is recovered at $t = \pi/|c|$.

One period of evolution of the initial edge state prepared at $k_1 = 0.375K$, i.e., of $\boldsymbol{\Psi}(\boldsymbol{r}, 0) = \boldsymbol{\psi}_1(\boldsymbol{r})$ shown in Figs. 1(c) and 1(d), at the exact Bragg resonance is presented in Fig. 3 in the real and in momentum spaces (due to fast decay of the edge estate along the $x$ direction we used periodic boundary conditions also in $x$). The evolution of the internal structure of the wave due to conversion between the states is visible from the comparison of real-space distributions at half-period ($t = 640$) and at one period ($t = 1280$). In the momentum space both spinor components of the state 1 at $t = 0$ and at $t = 1280$ (after one period) are localized mainly near two symmetric $K'$ points of the Brillouin zone [Fig. 3(f) shows the dominant first component]. The interference of both edge states is illustrated at a quarter-period, $t = 320$, in Fig. 3(a) in the real space and Fig. 3(d) in the momentum space. We observe spots of the spectral density in all $K$ and $K'$ points. After a half-period the Fourier transform of $\Psi^{(1)}$ (denoted by $\varphi^{(1)}$) is localized in the vicinity of $K$ points [Fig. 3(e)], with the upper $K$ point being more populated than the other two.

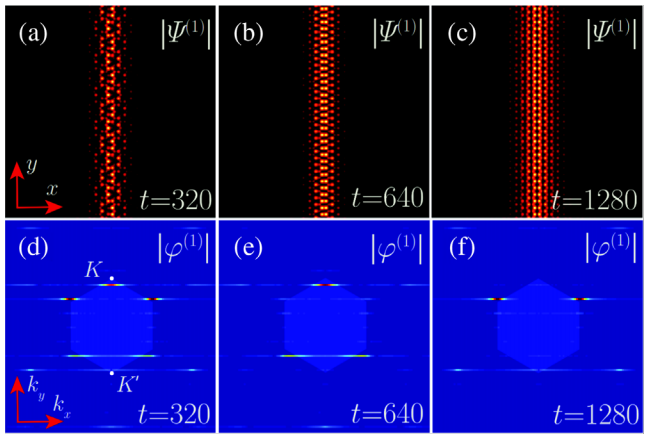


FIG. 3. Resonant scattering of the initial edge state prepared at $k_1 = 0.375K$ for $\delta = 0.004$. Real-space $|\Psi^{(1)}|$ distribution within $x, y \in [-16L, 16L]$ window (top row), and corresponding momentum-space $|\varphi^{(1)}|$ distribution within $k_x$, $k_y \in [-1.5K, 1.5K]$ window (bottom row) are shown at approximately a quarter-period ($t = 320$), half-period ($t = 640$), and one period ($t = 1280$).

The evolution of the densities $\nu_{1,2}$ for a near-resonant case $\Delta k \neq 0$, $\Delta\varepsilon \neq 0$ is illustrated in Fig. 2(b). We observe a weakening of the conversion and increase of the frequency of oscillations with an increase of the mismatch $\Delta k$. This can be understood by considering a plane-wave solution of Eq. (2): $a_j(t) = b_j e^{i\omega t - i(-1)^j(\Delta k y - \Delta\varepsilon t)/2}$, for which two frequencies are obtained: $\omega_\pm = \Delta k(v_2 - v_1)/4 \pm \{[(v_1 + v_2)\Delta k/2 - \Delta\varepsilon]^2/4 + c^2\}^{1/2}$. Thus, the period of the energy exchange between the states is $T = 2\pi/(\omega_+ - \omega_-)$. The energy difference $\Delta\varepsilon$ and coupling coefficient $c$ depend on the mismatch $\Delta k$ [see Fig. 4(a)]. The dependence of the maximal (over the whole time interval) density of the second edge state on momentum mismatch has a resonance character, as shown in Fig. 4(b). The exact resonance corresponding to complete transition between the edge states is achieved at $k_2 - k_1 \approx 0.2K$ and $\Delta\varepsilon = 0$.

In the nonlinear case Eq. (2) admits a Bragg-soliton solution. We write it for $g < 0$ and $c > 0$, and for the exact Bragg resonance $\Delta k = \Delta\varepsilon = 0$:

$$(a_1, a_2) = \frac{\sqrt{2c}\tau \sin\sigma}{\sqrt{|g|(\tau^8\chi_2 + 2\tau^4\tilde{\chi} + \chi_1)}} e^{i\varphi + i\eta} \times [\mathrm{sech}(\xi + i\sigma/2), \tau^2 \mathrm{sech}(\xi - i\sigma/2)], \quad (3)$$

where $\zeta_j = y - v_j t$,

$$\xi = \frac{c(\tau^4\zeta_2 + \zeta_1)\sin\sigma}{\tau^2(v_2 - v_1)}, \qquad \varphi = \frac{c(\tau^4\zeta_2 - \zeta_1)\cos\sigma}{\tau^2(v_2 - v_1)},$$
$$\eta = \frac{2(\tau^8\chi_2 - \chi_1)}{\chi_1 + 2\tilde{\chi}\tau^4 + \chi_2\tau^8} \arctan\left(\frac{1 - \cos\sigma}{\sin\sigma}\tanh\xi\right),$$

and $\sigma \in (0, \pi/2)$ and $\tau \in (-1, 1)$ remain free parameters. Such solitons move with the velocity of the envelope, i.e., $v_{\mathrm{sol}} = (\tau^4 v_2 + v_1)/(1 + \tau^4)$ (Bragg solitons for nontopological nonlinear optics were first found in [21,22]). Notice that azimuthal, $\theta = 2\sigma$, and polar, $\phi = \arccos\tau$, angles map the soliton to the unit Bloch sphere encoding information in the soliton in the same way as in a qubit.

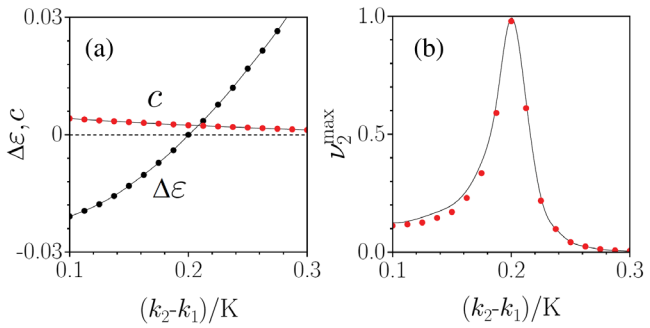


FIG. 4. (a) Energy mismatch $\Delta\varepsilon$, coupling constant $c$, and (b) maximal density $\nu_2^{\max}$ versus $k_2 - k_1$ at $k_1 = 0.375K$ and $\delta = 0.004$. Dots in (a) are guides for the eye. Dots in (b) show the results of direct simulations of Eq. (1) while the solid line shows predictions of the coupled-mode theory. The exact Bragg resonance occurs at $\kappa = 0.2K$.

Although Eq. (3) describes the 1D field distribution along the interface, the Bragg solitons reported here are 2D objects localized along and across the interface by different physical mechanisms. Therefore, now we turn to the results of direct numerical simulations of Eq. (1). Figure 5 shows the propagation of a topological Bragg soliton [panels (d)–(f)] in a condensate with a negative scattering length in comparison with dispersive dynamics of the same initial wave packet in a condensate without interatomic

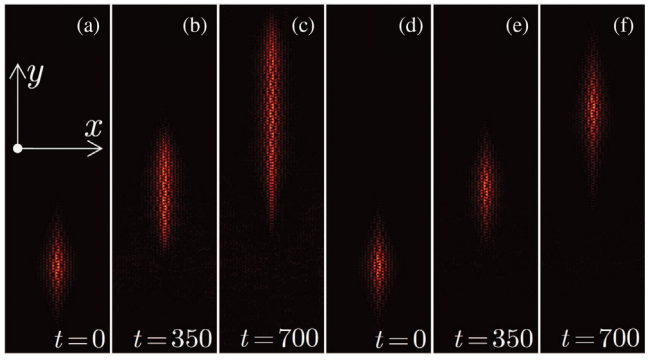


FIG. 5. $|\Psi^{(1)}|$ distributions of a wave packet at $g = 0$ (a)–(c) and a topological Bragg soliton at $g = -1$ (d)–(f), obtained by the direct simulation of (1) are shown at instants within the $x \in [-16L, 16L]$, $y \in [-60L, 60L]$ window. Initial distributions were constructed using (3) with $\tau = 1$, $\sigma = 0.44\pi$. The modulation amplitude $\delta = 0.008$ corresponds to $c = 0.00484$. The coupled modes have group velocities $v_1 = 0.2543$ and $v_2 = 0.1215$. We mention high accuracy of the definition of the soliton velocity, which is 0.1828 in the shown numerical results, as compared to 0.1879 predicted by (3). The nonlinear coefficients are $\chi_1 = 0.0739$, $\chi_2 = 0.1515$, and $\tilde{\chi} = 0.1965$.

interactions [panels (a)–(c)]. We observe the robustness of the Bragg soliton, which is topologically protected from the energy losses into other modes of the system, that also illustrates a high accuracy of formula (3) for the soliton shape. The soliton is confined at the interface due to its topological nature; hence it is quasi-1D and it is also protected against collapse, although the system is 2D and the interactions are attractive. The weak broadening of the soliton visible at large times $t \sim 700$ is attributed to higher-order dispersion which is not accounted for by the model (2).

Summarizing, weak periodic perturbation at the interface between two topologically different media with two or more edge states enables resonant transitions between them. This allows the manipulation of edge states, their selective excitation, and control of their propagation velocity. Because of the topological nature of the system, Bragg scattering channels are limited to the edge-state subspace, remaining immune to scattering into bulk modes. When the system bears nonlinearity, it supports the propagation of topological Bragg solitons inheriting topological protection from the modes on which they are constructed. Robustness, dynamical nature, and parametrization make Bragg solitons good candidates for the implementation of qubits. Our results are not limited to atomic states described here; they can be observed in any system supporting more than one topological state per interface. Furthermore, they pave a way to the investigation of a plethora of multiwave processes involving edge states, three-wave processes and four-wave mixing being among them. They also indicate the possibilities of other coupling mechanisms such as, for example, Bragg scattering on phonons.

Y. V. K. acknowledges the funding of this study by RFBR and DFG according to research Project No. 18-502-12080. V. V. K. was supported of the FCT (Portugal) under Grant No. UID/FIS/00618/2019. W. Z. and F. Y. acknowledge the support of NSFC (No. 91950120, No. 11690033, and No. 61475101) and of the Natural Science Foundation of Shanghai (No. 19ZR1424400).

*Corresponding author.
fangweiye@sjtu.edu.cn

[1] B. I. Halperin, Quantized Hall conductance, current-carrying edge states, and the existence of extended states in a two-dimensional disordered potential, Phys. Rev. B **25**, 2185 (1982).

[2] Y. Hatsugai, Chern Number and Edge States in the Integer Quantum Hall Effect, Phys. Rev. Lett. **71**, 3697 (1993).

[3] F. D. M. Haldane, Model for a Quantum Hall Effect without Landau Levels: Condensed-Matter Realization of the Parity Anomaly, Phys. Rev. Lett. **61**, 2015 (1988); Z. Qiao, S. A. Yang, W. Feng, W.-K. Tse, J. Ding, Y. Yao, J. Wang, and Q. Niu, Quantum anomalous Hall effect in graphene from Rashba and exchange effects, Phys. Rev. B **82**, 161414 (2010); C.-Z. Chang, J. S. Zhang, X. Feng, J. Shen, Z. C. Zhang, M. H. Guo, K. Li, Y. Ou, and P. Wei, Experimental observation of the quantum anomalous Hall effect in a magnetic topological insulator, Science **340**, 167 (2013).

[4] C. L. Kane and E. J. Mele, Quantum Spin Hall Effect in Graphene, Phys. Rev. Lett. **95**, 226801 (2005); L. Sheng, D. N. Sheng, C. S. Ting, and F. D. M. Haldane, Nondissipative Spin Hall Effect via Quantized Edge Transport, Phys. Rev. Lett. **95**, 136602 (2005).

[5] C. L. Kane and E. J. Mele, $Z2$ Topological Order and the Quantum Spin Hall Effect, Phys. Rev. Lett. **95**, 146802 (2005).

[6] M. Z. Hasan and C. L. Kane, Colloquium: Topological insulators, Rev. Mod. Phys. **82**, 3045 (2010); X.-L. Qi and S.-C. Zhang, Topological insulators and superconductors, Rev. Mod. Phys. **83**, 1057 (2011).

[7] A. Y. Kitaev, Unpaired Majorana fermions in quantum wires, Phys. Usp. **44**, 131 (2001).

[8] F. D. M. Haldane and S. Raghu, Possible Realization of Directional Optical Waveguides in Photonic Crystals with Broken Time-Reversal Symmetry, Phys. Rev. Lett. **100**, 013904 (2008); S. Raghu and F. D. M. Haldane, Analogs of quantum-Hall-effect edge states in photonic crystals, Phys. Rev. A **78**, 033834 (2008).

[9] S. A. Skirlo, L. Lu, and M. Soljačić, Multimode One-Way Waveguides of Large Chern Numbers, Phys. Rev. Lett. **113**, 113904 (2014).

[10] Z. Wang, Y. Chong, J. D. Joannopoulos, and M. Soljačić, Observation of unidirectional backscattering-immune topological electromagnetic states, Nature (London) **461**, 772 (2009).

[11] A. B. Khanikaev, S. H. Mousavi, W. K. Tse, M. Kargarian, A. H. MacDonald, and G. Shvets, Photonic topological insulators, Nat. Mater. **12**, 233 (2013); F. Gao, H. R. Xue, Z. J. Yang, K. F. Lai, Y. Yu, X. Lin, Y. D. Chong, G. Shvets, and B. L. Zhang, Topologically protected refraction of robust kink states in valley photonic crystals, Nat. Phys. **14**, 140 (2018).

[12] L. Lu, J. D. Joannopoulos, and M. Soljačić, Topological photonics, Nat. Photonics, **8**, 821 (2014); A. B. Khanikaev and G. Shvets, Two-dimensional topological photonics, Nat. Photonics **11**, 763 (2017).

[13] K. Y. Bliokh, D. Smirnova, and F. Nori, Quantum spin Hall effect of light, Science **348**, 1448 (2015).

[14] N. Goldmana, J. Dalibard, A. Dauphina, F. Gerbierb, M. Lewensteine, P. Zoller, and I. B. Spielman, Direct imaging of topological edge states in cold-atom systems, Proc. Natl. Acad. Sci. U.S.A. **110**, 6736 (2013); J. Jüemann, A. Piga, S.-J. Ran, M. Lewenstein, M. Rizzi, and A. Bermudez, Exploring Interacting Topological Insulators with Ultracold Atoms: The Synthetic Creutz-Hubbard Model, Phys. Rev. X **7**, 031057 (2017).

[15] B. Galilo, D. K. K. Lee, and R. Barnett, Topological Edge-State Manifestation of Interacting 2D Condensed Boson-Lattice Systems in a Harmonic Trap, Phys. Rev. Lett. **119**, 203204 (2017).

[16] H. Zhai, M. Rechtsman, Y.-M. Lu, and K. Yang, Focus on topological physics: From condensed matter to cold atoms and optics, New J. Phys. **18**, 080201 (2016).

[17] C. Li, F. Ye, X. Chen, Y. V. Kartashov, L. Torner, and V. V. Konotop, Topological edge states in Rashba-Dresselhaus spin-orbit-coupled atoms in a Zeeman lattice, Phys. Rev. A **98**, 061601(R) (2018).

[18] A. V. Nalitov, D. D. Solnyshkov, and G. Malpuech, Polariton $Z$ Topological Insulator, Phys. Rev. Lett. **114**, 116401 (2015); T. Karzig, C.-E. Bardyn, N. H. Lindner, and G. Refael, Topological Polaritons, Phys. Rev. X **5**, 031001 (2015); Y. Zhang, Y. V. Kartashov, Y. Zhang, L. Torner, and D. V. Skryabin, Resonant edge-state switching in polariton topological insulators, Laser Photonics Rev. **12**, 1700348 (2018); S. Klembt, T. H. Harder, O. A. Egorov, K. Winkler, R. Ge, M. A. Bandres, M. Emmerling, L. Worschech, T. C. H. Liew, M. Segev, C. Schneider, and S. Hofling, Exciton-polariton topological insulator, Nature (London) **562**, 552 (2018).

[19] Y. V. Kartashov and D. V. Skryabin, Modulational instability and solitary waves in polariton topological insulators, Optica **3**, 1228 (2016).

[20] J. Li, J. Lee, W. Huang, S. Burchesky, B. Shteynas, F. C. Top, A. O. Jamison, and W. Ketterle, A stripe phase with supersolid properties in spin-orbit-coupled Bose Einstein condensates, Nature (London) **543**, 91 (2017).

[21] D. N. Christodoulides and R. I. Joseph, Slow Bragg Solitons in Nonlinear Periodic Structures, Phys. Rev. Lett. **62**, 1746 (1989).

[22] A. B. Aceves and S. Wabnitz, Self-induced transparency solitons in nonlinear refractive periodic media, Phys. Lett. **141A**, 37 (1989).

[23] G. P. Agrawal, *Applications of Nonlinear Fiber Optics* (Academic Press, San Diego, 2008).

[24] Y. J. Lin, K. Jiménez-García, and I. B. Spielman, Spin-orbit-coupled Bose-Einstein condensates, Nature (London) **471**, 83 (2011).

[25] V. Galitski and I. B. Spielman, Spin-orbit coupling in quantum gases, Nature (London) **494**, 49 (2013).

[26] G. Grynberg, B. Lounis, P. Verkerk, J.-Y. Courtois, and C. Salomon, Quantized Motion of Cold Cesium atoms in Two- and Three-Dimensional Optical Potentials, Phys. Rev. Lett. **70**, 2249 (1993).

[27] P. Soltan-Panahi, D.-S. Lühmann, J. Struck, P. Windpassinger, and K. Sengstock, Quantum phase transition to unconventional multi-orbital superfluidity in optical lattices, Nat. Phys. **8**, 71 (2012).

[28] S. Lopez-Aguayo, Y. V. Kartashov, V. A. Vysloukh, and L. Torner, Method to Generate Complex Quasinondiffracting Optical Lattices, Phys. Rev. Lett. **105**, 013902 (2010); A. Ortiz-Ambriz, S. Lopez-Aguayo, Y. V. Kartashov, V. A. Vysloukh, D. Petrov, H. Garcia-Gracia, J. C. Gutiérrez-Vega, and L. Torner, Generation of arbitrary complex quasi-non-diffracting optical patterns, Opt. Express **21**, 22221 (2013).

[29] K. Jiménez-García, L. J. LeBlanc, R. A. Williams, M. C. Beeler, A. R. Perry, and I. B. Spielman, Peierls Substitution in an Engineered Lattice Potential, Phys. Rev. Lett. **108**, 225303 (2012).

[30] M. C. Rechtsman, J. M. Zeuner, Y. Plotnik, Y. Lumer, D. Podolsky, F. Dreisow, S. Nolte, M. Segev, and A. Szameit, Photonic Floquet topological insulators, Nature (London) **496**, 196 (2013).

[31] M. J. Ablowitz and Y. Zhu, Evolution of Bloch-mode envelopes in two-dimensional generalized honeycomb lattices, Phys. Rev. A **82**, 013840 (2010).

[32] E. Zhao and A. Paramekanti, BCS-BEC Crossover on the Two-Dimensional Honeycomb Lattice, Phys. Rev. Lett. **97**, 230404 (2006); Z. Chen and B. Wu, Bose-Einstein Condensate in a Honeycomb Optical Lattice: Fingerprint of Superfluidity at the Dirac Point, Phys. Rev. Lett. **107**, 065301 (2011).

[33] E. I. Rashba, Properties of semiconductors with an extremum loop: 1. Cyclotron and combinational resonance in a magnetic field perpendicular to the plane of the loop, Fiz. Tverd. Tela **2**, 1224 (1960) [Sov. Phys. Solid State **2**, 1109 (1960)].

[34] G. Dresselhaus, Spin-orbit coupling effects in zinc blende structures, Phys. Rev. **100**, 580 (1955).

[35] See Supplemental Material at http://link.aps.org/supplemental/10.1103/PhysRevLett.123.254103 for the derivation of the coupled mode equations used in the main text.